Gravity Wave Weakening During the 2019 Antarctic Stratospheric Sudden Warming

Masaru Kogure[1], Jia Yue[2,3], Huixin Liu[1]

[1]Department of Earth and Planetary Science, Kyushu University, 744 Motooka Nishi-ku, Fukuoka, Japan. [2]NASA Goddard Space Flight Center, 8800 Greenbelt Rd, Greenbelt, MD, USA. [3]Catholic University of America, 620 Michigan Ave NE, Washington, DC, USA

Corresponding author: Masaru Kogure (kogure.masaru.695@m.kyushu-u.ac.jp)

Key Points:

- Gravity waves at 20–70 km altitudes decreased after the onset of the 2019 Antarctic stratospheric sudden warming.
- The decline of gravity wave activities coincided with the weakening of zonal wind.
- The decline in gravity wave activities was caused by wind filtering, wave saturation, and disruption of the polar night jet.

Abstract

The Antarctic stratospheric sudden warming (SSW) occurred on August 30, 2019, and was a vortex displacement minor warming event. We investigated variations in gravity waves (GWs) before and after this rare Antarctic SSW event using two satellite measurements (AIRS and CIPS) and reanalysis data (GEOS-5 FP). The observations showed that the GW activities decreased after the SSW onset, with a weakening of zonal wind. The decrease in GW activity coincided with a reversal of the zonal wind around September 8 in GEOS-5 FP. The temporal variation of GWs was similar to that of Arctic GWs during vertex displacement minor SSWs. The decline in GW activities was probably caused by wind filtering and polar night jet breaking. However, the GW activities over the Andes and the Antarctic peninsula decreased at the onset, although the westly wind was 40–60 ms^{-1}. This decrease could have been caused by wave saturation.

Plain Language Summary

The strong west wind, called the polar night jet, appears in the winter polar region and typically exceeds 90 ms^{-1} at its maximum. The temperature inside the jet (the polar vortex) is colder than that outside the jet. However, the polar night jet occasionally becomes highly distorted and disappears with accompanying warming in the polar stratosphere. Such events are called sudden stratospheric warmings (SSWs). SSWs drastically change the wind and temperature, which should strongly influence small-scale waves, called gravity waves (GWs). SSWs frequently occur in the Arctic, but rarely in the Antarctic. Antarctic SSWs have occurred only twice in the 21st century. The rare Antarctic SSWs occurred in 2019, and we investigated GW variations before/after the SSW event. A decline in GW activity coincided with a decline in the zonal wind twice in GEOS-5 FP. The decline in GW activity was probably caused by a weak zonal wind layer. This temporal variation is the same as the Arctic GWs for the same type of SSW.

1 Introduction

The winter polar stratosphere is characterized by a strong westly wind, i.e., the polar night jet (Chandran et al., 2014). The polar night jet exceeds 90 ms^{-1}, and the temperature inside the jet (the polar vortex) is colder than that outside the jet (Fleming et al., 1990). However, the polar night jet occasionally becomes highly distorted and sometimes disappears with accompanying warming. Such events are called sudden stratospheric warmings (SSWs). SSWs are triggered by enhanced propagation of wavenumber 1 or 2 planetary waves from the troposphere, and planetary wave

breaking decelerates the polar night jet and sometimes reverses the zonal wind (Chandran et al., 2014).

The World Meteorological Organization classifies SSWs into two categories: minor and major warmings. During minor warmings, the zonal mean temperature at the pole is higher than that at 60°N at 10 hPa. During a major warming, the zonal wind reverses from a westly wind to an eastly wind at 10 hPa, in addition to higher temperatures at the pole (Chandran et al., 2014). Furthermore, SSWs can be categorized by their zonal structures, polar vortex displacement, or splitting events (Charlton & Polvani, 2007; Matthewman et al., 2009). During a vortex displacement event, the vortex moves out of the pole and tilts westward with height, with an enhanced wavenumber 1 planetary wave. During a vortex splitting event, the vortex splits into two or more cyclonic cells, with an enhanced wavenumbers 2 planetary wave.

Because SSWs drastically change the meteorological field in the middle atmosphere, gravity wave (GW) generation and propagation are consequently altered. Arctic SSWs frequently occur such that the SSW effects on GWs in the northern hemisphere have been well studied. Ern et al. (2016) investigated temporal Arctic GW variations before and after the SSW onsets from 2001 to 2014. They showed that GW activities were strongly suppressed when zonal wind became reversed after a SSW onset. Before the onset, the GW activities were enhanced only during major warmings and split vortex events. This enhancement could be caused by the enhanced imbalance flow. These characteristics of Arctic GWs during SSWs have been supported by models and observational studies (Jia et al. 2015; Wang & Alexander, 2009; Wright et al., 2010; Yamashita et al., 2010, 2013). On the other hand, Antarctic SSWs have occurred only twice in the 21st century (2002 and 2019). Most satellite observations of GWs became available after 2000. The 2002 Antarctic SSW was a vortex splitting major warming event (Baldwin et al., 2003). Ratnam et al. (2004) used CHAMP/GPS occultation measurements to determine that the enhancement and decline of Antarctic GWs occurred before and after, respectively, SSW onset. This was consistent with the Arctic vortex splitting major warming events. The 2019 Antarctic SSW occurred around August 30 and was led by the enhancement of planetary waves with zonal wavenumber 1 (Yamazaki et al., 2020). Although this 2019 SSW event was classified as a minor warming event, the zero zonal wind layer reached a 40 km altitude. This wind variation could influence GWs in the southern hemisphere. The objective of this study was to reveal temporal and spatial GW variations in the southern hemisphere before and after the 2019 Antarctic SSW event.

2 Analysis and data

2.1 GEOS-5 FP

The GW perturbations and absolute momentum fluxes during the Antarctic 2019 SSW were estimated with the GEOS-5 FP (Forward Processing) reanalysis data (Lucchesi, 2013). The GEOS-5 FP is a global non-hydrostatic, high horizontal resolution ($0.3125°$ longitude $\times$ $0.25°$ latitude) simulation, and is assimilated with observations. The GEOS-5 FP is the three-hourly interval instantaneous product and has 72 vertical levels from the surface to 0.01 hPa (~80 km altitude). The vertical resolution was ~2 km in the middle atmosphere. The three top layers (0.01–0.04 hPa) are strong sponge layers; therefore, GWs were derived below 0.05 hPa (~70 km altitude). The orographic and non-orographic GW parameterizations (Garcia & Boville, 1994; McFarlane, 1987) are also used in the GEOS-5 FP; however, in this study, we focused on resolved GWs in the GEOS-5 FP, that is, the GWs with horizontal and vertical wavelengths longer than ~100 km and ~4 km, respectively. Holt et al. (2017) evaluated GWs resolved by a model producing the GEOS-5 FP (GEOS-5) in the Southern Hemisphere. They used the GEOS-5 Nature Run, which was produced by the high-resolution GEOS-5 model but was not assimilated by any observations. The GWs in the GEOS-5 display realistic global patterns in their amplitude, absolute momentum flux, and horizontal wavelength, although their amplitudes are approximately four times weaker than the observations. Thus, the GEOS-5 model can resolve mesoscale GWs, including non-orographic waves.

To derive GW perturbations, the background field in the GEOS-5 FP was defined as a spherical harmonic series truncated at horizontal wavenumber $n = 40$, which is equivalent to ~1000 km horizontal wavelength, according to Holt et al. (2017). The GW perturbations were then obtained by subtracting the background. Thus, we derived GWs with horizontal wavelengths less than ~1000 km. From the perturbations and background, the daily mean absolute GW momentum flux, *M*, was estimated as in eq. (1) in Geller et al. (2013).

2.2 Atmospheric Infrared Sounder (AIRS)

The AIRS instrument aboard the NASA Aqua satellite (Aumann et al., 2003; Chahine et al., 2006) measures infrared radiance spectra between 3.74 and 15.4 μm. To investigate GWs, 15 μm brightness temperature data averaged over two sets of AIRS channels were used and compared with the GWs in GEOS-5 FP. The two channel sets were used for averaging, with temperature kernel functions peaking in two layers at ~23 and ~40 km altitudes. The full widths at half maximum of

the kernel functions are typically ~15 km and therefore represent mean temperatures over 17–32 and 34–49 km altitudes, respectively. Second, a fourth-order polynomial fit was subtracted for each across-track scan to remove the backgrounds. The remaining temperature perturbations provided a measure of GWs with vertical wavelengths longer than ~15 km and ~30–500 km horizontal wavelengths. The AIRS/Aqua observations of GWs are described in detail by Hoffmann et al. (2013, 2017).

2.3 Cloud Imaging and Particle Size instrument (CIPS)

The CIPS on the NASA Aeronomy of Ice in the Mesosphere satellite (AIM) (McClintock et al., 2009; Rusch et al., 2009) is a nadir-viewing panoramic imager that observes ultraviolet radiation (265 nm) scattered by Rayleigh scattering and polar mesospheric clouds (PMCs). In the absence of PMCs (including the Antarctic region during austral winter), the Rayleigh scattering source function at the 265 μm radiance peaks at altitudes of 50–55 km, with its full widths at a half maximum altitude of ~15 km (Bailey et al., 2009).

The Rayleigh scattering Albedo Anomaly (RAA) observed by CIPS corresponds to GW density (temperature) relative perturbations (Randall et al., 2017). To calculate RAA, a background Rayleigh albedo was calculated using a numerical generalization of the "$C - \sigma$" model, which was described by Carstens et al. (2013). The RAA observed by CIPS is most sensitive to GWs at ~52 km, with vertical wavelengths longer than ~15 km and ~15–600 km horizontal wavelengths. RAA retrieval was described by Randall et al. (2017).

3 Time variation of GW temperature perturbation in AIRS and CIPS observations and the GEOS 5-FP model

Figure 1 shows the GWs temperature perturbations observed by AIRS (CIPS) and GEOS-5 FP. To compare observations with model simulations, the perturbations in the GEOS-5 FP were averaged with AIRS and CIPS observational vertical kernels. The GW perturbations at 40 and 52 km before the SSW onset (August 24) were large over the Andes, the Antarctic peninsula (where are well known as orographic GW hot spots (Hoffmann et al., 2013)), and the Southern Ocean. The GW enhancement area over the Southern Ocean corresponded to a strong zonal wind region, i.e., the polar night jet. This suggests that the polar night jet was the source of these GWs. The GW perturbations after the SSW onset (September 3 and 13) were much weaker than those on August 24. Daily mean zonal wind in GEOS-5 FP also decreased after SSW onset at 40 km and 52 km. The

vortex moved out of the pole toward the Andes, because the 2019 Antarctic SSW was a vortex displacement event. The GWs on September 3 still appeared in the polar night jet, but the GWs almost disappeared on September 13. Accompanying the decline of the perturbations, the mean zonal wind was weakened and changed to an eastly wind, although the local zonal wind around the Andes was still a ~30–60 m s^{-1} westly wind. The GW perturbations at a 23 km altitude also decreased similar to those at 40 and 52 km, although the polar night jet remained (see Figures S1 in Supporting Information). Thus, the GW activity decreased after SSW onset. Such a decline in the GWs during Arctic SSWs is well known and can be explained by two mechanisms: (1) wind filtering of GWs with small zonal phase velocities because of wind reversal (Ratnam et al., 2004; Yamashita et al., 2010), (2) weakening or even the disappearance of the GW sources, i.e., the polar night jet (Yamashita et al., 2010). Moreover, there is a possibility that an observational filter was applied because of the shortened vertical wavelengths (Alexander, 1998). AIRS and AIM cannot capture GWs with vertical wavelengths shorter than ~15 km. However, GWs with short vertical wavelengths tend to be dissipated by eddy diffusion and instability, even though the GWs may not break (Lindzen et al., 1981). It should be noted in Figure 1 that the amplitudes of the GWs in the observations were approximately three times larger than those in the model. Although the observations and the model are sensitive to GWs with shorter and longer wavelengths, respectively, the GWs with longer wavelengths typically have larger amplitudes than shorter ones (Fritts & Alexander, 2003). This underestimation of the amplitude in the GEOS-5 model has been reported by Holt et al. (2016; 2017) and is caused by the excessive dissipation because of the coarser vertical resolution. This is common in many general circulation models (Jewtoukoff et al., 2015).

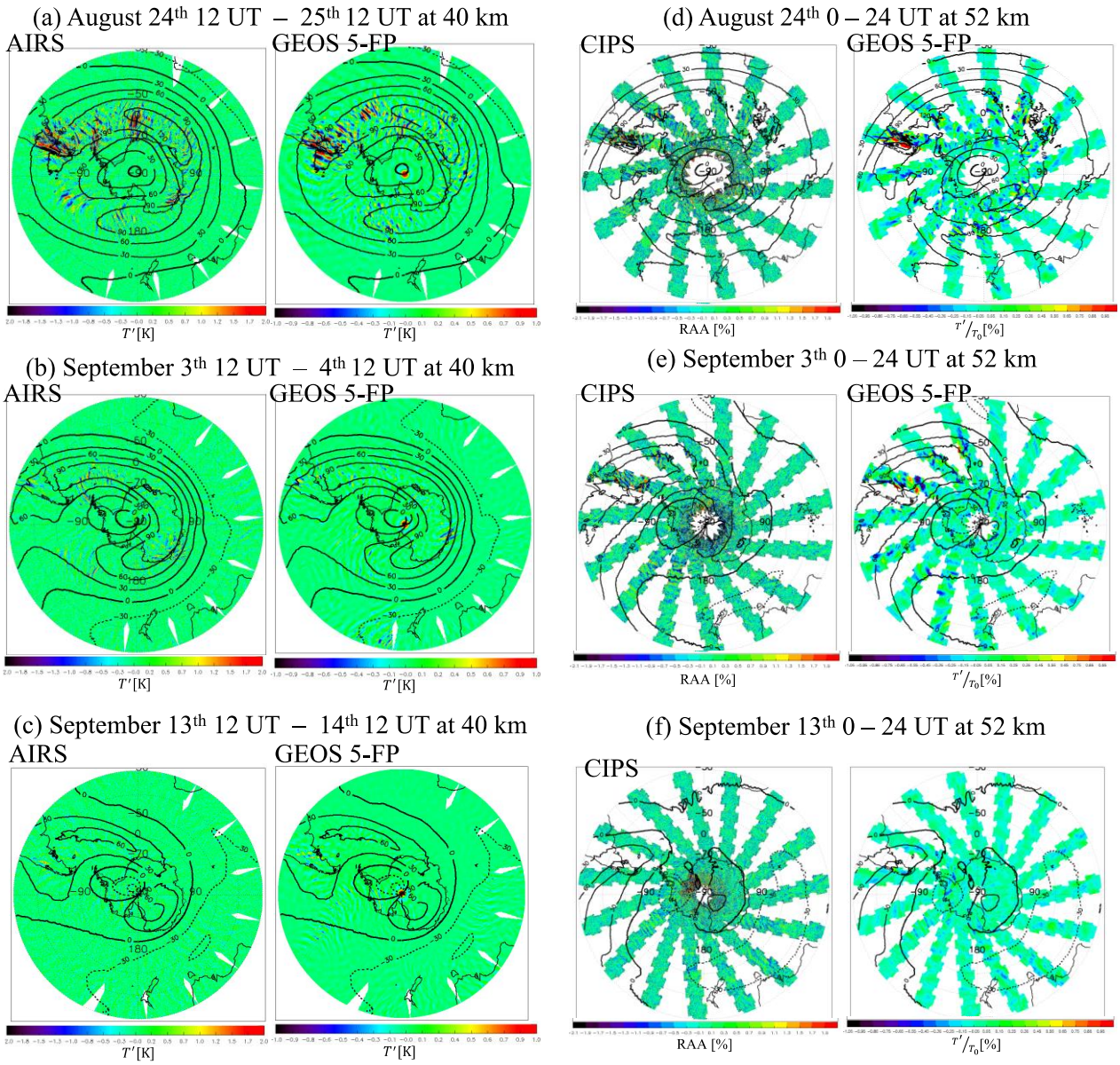

Figure 1. Gravity wave temperature perturbations for AIRS, CIPS, and GEOS-5 FP in the Southern hemisphere ($30 - 90°$S). Graphs a–c show the perturbations at a 40 altitude km from 12 UT on August 24 to 12 UT on August 25, from 12 UT on September 3 to 12UT on September 4, and from 12 UT on September 13 to 12 UT on September 14, respectively. Graphs d–f show relative temperature (density) perturbations at a ~52 km on August 24 at 0–24 UT, September 3 at 0–24 UT, and September 13 at 0–24 UT, respectively. The contour lines indicate daily mean zonal wind obtained from GEOS-5 FP. Thick lines and dotted lines indicate 0 m s^{-1} and an eastly wind, respectively.

Nevertheless, the GWs in GEOS-5 FP are in good agreement with the satellite observations in terms of their spatial and temporal variations. GEOS-5 FP can provide the tendency and behavior of GWs that is more accurate than the observations. We focus on the GWs in GEOS-5 FP during the Antarctic SSW in the following section. Additionally, the analysis of GEOS-5 FP is immune to observational filtering problems.

4 Temporal and special variations of absolute GW momentum fluxes in GEOS-5 FP before and after the Antarctic 2019 SSW

Figures 2 (a) and (b) show the zonal mean absolute GW momentum flux averaged at 50–70 °S during 2018 and 2019, respectively. No Antarctic SSW occurred in 2018, and the flux in 2018 was typical and is shown as a reference. The flux in the 55–70 km altitudes during 2018 declined by one-quarter from September 7 to September 19, with a ~20 ms^{-1} decrease in the westly zonal wind. The flux at ~10–45 km altitudes did not change. However, the flux in 2019 before the onset was comparable with that in 2018 and did not increase. After the onset, the flux at the 30–70 km altitudes on August 31 decreased by half of that during 20–29 August. The flux in the upper stratosphere on 12–19 September was one-seventh smaller than that during 20–30 August (e.g., 2.2×10^{-6} Pa at 50 km during 20–30 August but 3.0×10^{-7} Pa during 12–19 September). The flux at 20–30 km altitudes decreased by half, as well. The zonal wind became weaker above ~25 km at the SSW onset but there was still a westly wind. On September 5 the zero zonal wind line dropped to an ~40 km altitude (3 hPa).

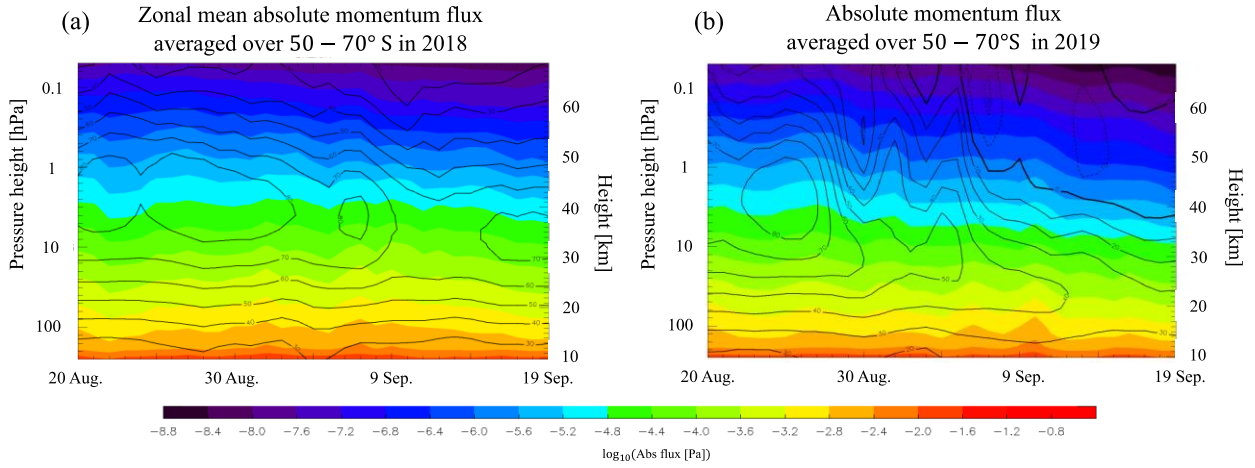

Figure 2. Daily mean absolute momentum fluxes in GEOS 5-FP over $50 - 70°S$. Graphs a and b show the zonal mean fluxes in 2018 and 2019, respectively. Contour lines indicate daily mean zonal wind. Thick, solid, and dotted lines indicate a 0 ms^{-1}, westly, and eastly wind, respectively.

Such coincidence in wind and flux decreases is common after a SSW onset (Thurairajah et al., 2014; Yamashita et al., 2010), and the decrease in GW fluxes was caused by the weakening and breaking of the polar night jet, that is, a lack of the GW source and wind filtering by the GWs with small ground-based zonal phase velocity. This temporal variation was different from the 2002 Antarctic splitting vortex SSW, because no GW enhancement occurred before the SSW onset, (Ratnam et al., 2004), but was similar to the Arctic GWs during vortex displacement minor SSWs (Ern et al., 2016). Thus, the imbalance in flow area did not increase with the 2019 SSW.

To investigate the spatial variations in the absolute GW momentum fluxes, we calculated the fluxes averaged over three periods: before the SSW onset (20–30 August), after the SSW but while the zonal wind was still westly at a 40 km altitude (August 31–September 8), and when the zonal wind was eastly at a 40 km altitude (9–19 September). Figures 3 shows the absolute GW momentum fluxes over 40–90 °S at 100, 10, 1, and 0.1 hPa (15, 30, 47, and 64 km) during the three periods, respectively. The fluxes on 20–30 August at each height had similar spatial variations during austral winter; that is, the fluxes were high around the polar night jet (50–70°S), the Andes, and the Antarctic peninsula (Preusse et al., 2009). Additionally, the high GW flux region over the Andes extended leeward (up to ~40°W). During August 31–September 8, the polar night jet above 10 hPa weakened and shrank, and the flux around the polar night jet decreased by approximately half. Between September 9–19, the flux at 100 hPa over the Southern Ocean (e.g., 50–60°S in the eastern hemisphere) was 0.4 times smaller than that before September 8. The zonal wind at 100 hPa also decreased by ~10 ms^{-1}, and this decrease in the GW activity could have been caused by the weaker source (the polar night jet). The polar night jet at 10 hPa weakened and shrunk more than that during August 31–September 8, and the jet disappeared at 1 hPa. At 0.1 hPa, the zonal wind was eastly, except in the vicinity of the Andes; however, it was small (10–20 ms^{-1}).

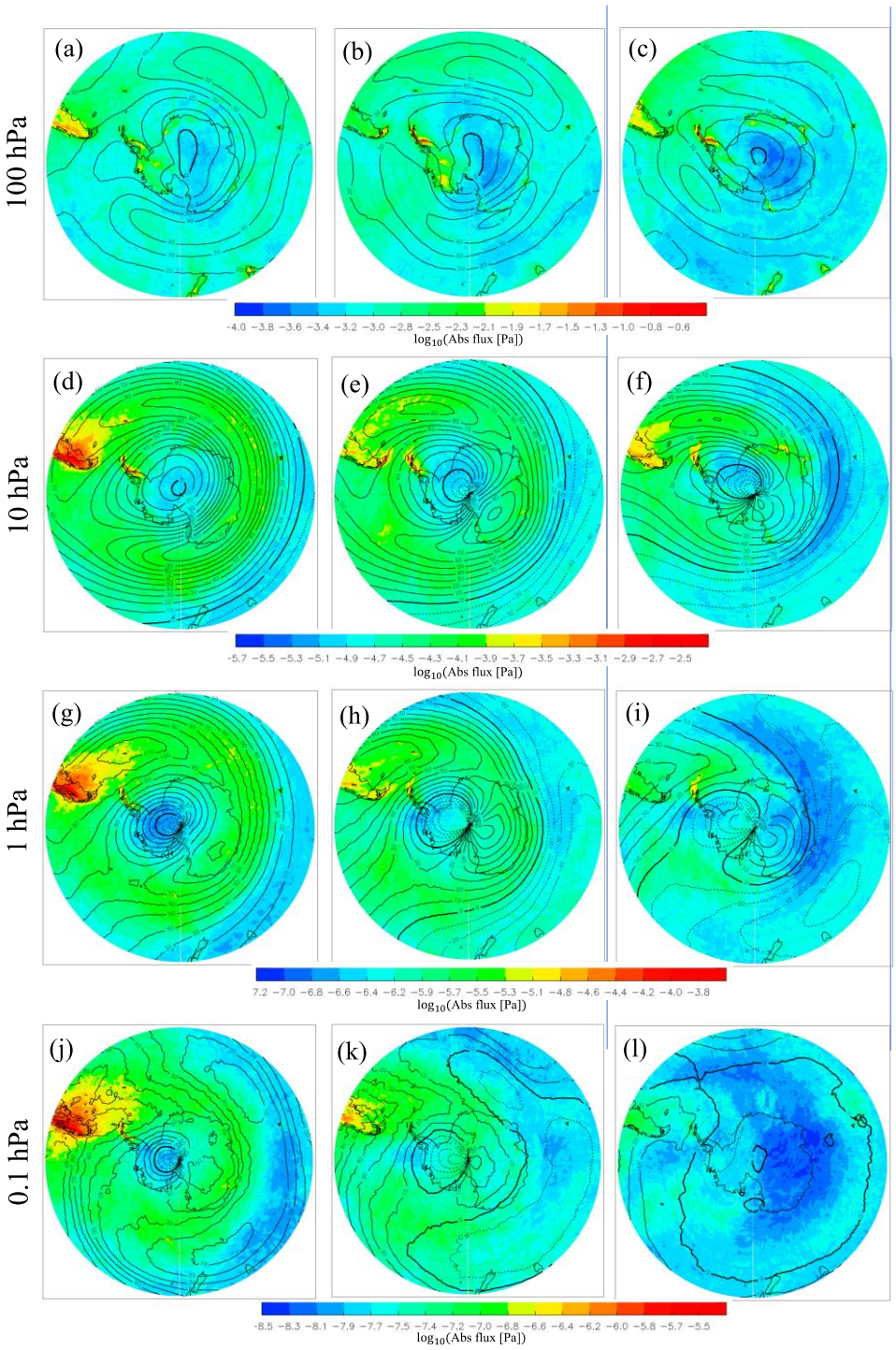

Figure 3. Absolute momentum fluxes averaged in GEOS 5-FP in the three periods: before/after the onset of the 2019 Antarctic SSW (August 20 to 30 and August 31 to September 8), and during the weak zonal wind in the middle/upper stratosphere (September 9 to 19). The contour lines indicate daily mean zonal wind. Thick lines and dotted lines indicate 0 ms^{-1} and an east wind, respectively. Graphs a–c show the averaged fluxes at 100 hPa. Graphs d–l) are the same as a–c, except for 10 hPa (d–f), 1 hPa (g–i), and 0.1 hPa (j–l), respectively.

Accompanying this weakening of the eastly wind, the flux dropped by 1–2 orders in the polar night jet region (50–60 °S), the Andes, and the Antarctic peninsula. It should be noted that the flux at 10 hPa (20–50 °E, 70°S) was enhanced during September 9–19. This area overlapped with an exit of the polar night jet, and consequently, the GWs could be emitted from the polar night jet through spontaneous adjustment (Plougonven & Zhang, 2014). Figures 3 shows that the zonal winds around the Andes and the Antarctic peninsula were mostly westly after the onset. However, the zonal wind over most regions of the Southern Ocean, especially in the eastern hemisphere, was eastly. Moreover, the mountains in the Andes and the Antarctic peninsula were the main source of the GWs, whereas the main sources of the GWs in the Southern Ocean were the fronts and the polar night jet (Hendricks et al., 2014; Murphy et al., 2014; Sato & Yoshiki, 2008). Thus, the behavior of the GWs and the background winds in both regions were different. We compare the GW fluxes between the orographic GW hotspots (the Andes and the Antarctic peninsula) and the Southern Ocean in this section.

Figures 4 (a) and (b) show the daily mean absolute momentum fluxes in GEOS-5 FP over 50–80°W, 50–70°S (the southern Andes and Antarctic peninsula) and 165°E–165°W, 50–70°S (hereinafter, this region is called the ocean region). The ocean region is far from any continent or island, and the polar night jet existed there before the onset (Figure 3 d and g), that is, non-orographic GWs mainly contributed to the flux there. The wind and flux over the ocean region were similar to the zonal mean values (e.g., zonal wind peak altitude and the time of the decline of the zonal wind and the flux), although the flux was one-half smaller than the zonal mean value. This is because most areas in 50–70°S are over the ocean. The flux over the southern Andes and Antarctic peninsula was 10–50% larger than the zonal mean value, especially in the lower stratosphere. This high flux was caused by mountain waves. The zonal winds over the southern Andes and Antarctic peninsula were higher (lower) at 10–35 (35–70) km altitudes than the zonal mean value. In terms of temporal variations, the zonal wind and flux in both regions decreased in two steps (the first step was the SSW onset, and the second was the drop in the zonal wind), although the second step over the ocean region was earlier than that over the southern Andes and Antarctic peninsula. The decreases in the zonal wind and flux coincided. This suggests that the fluxes were suppressed because of the wind reversal filtering GWs from the troposphere and the lack of a stratospheric GW source (the polar night jet). Although the zonal wind over the southern Andes and Antarctic peninsula was still strong (40–60 ms^{-1}) in the first step (onset) in the 40–60 km altitudes, the flux

256 decreased by half at 50 km. This implied that mountain waves were not filtered out by their critical
257 level. Additionally, the flux in the 10–20 km altitudes was larger between the first and second steps
258 than that before the first step, which suggested that the orographic source activity was higher. This
259 decrease in flux at the first step over the southern Andes and Antarctic peninsula could be explained
260 by the wave saturation because of the decrease in the zonal wind. The GWs around the polar night
261 jet tend to have long vertical wavelengths because of the Doppler shift. When the wind decreases,
262 the vertical wavelengths should likewise decrease. GWs with small vertical wavelengths have a
263 tendency to meet instability conditions, and the growth of the amplitudes is limited (Alexander et
264 al., 2011; Whiteway et al., 1997). Figures 4 c and d show the vertical wavelength spectra for the
265 GW relative temperature perturbation and wind over the southern Andes and Antarctic peninsula–
266 at 10–70 km from August 20 to August 30, August 31 to September 8, and September 9 to
267 September 19, respectively. Figures 4 e and f show the same values as c and d, except for the ocean
268 region. The spectra were calculated using the Lomb–Scargle method (Scargle, 1982). The power
269 spectral densities (PSDs) over the southern Andes and Antarctic peninsula at vertical wavelengths
270 longer than 20 km dropped to one-half to one-third from August 20–30 to August 31–September 8,
271 although shorter vertical wavelengths than 10 km decreased by less than two-thirds. The
272 characteristic vertical wavelength (local maximum wavelength) also became shorter (~20 km to
273 ~16 km). The PSDs over the ocean dropped to one-half to one-third for all vertical wavelengths,
274 and the characteristic vertical wavelength did not change. This result indicated that the GWs with
275 longer vertical wavelengths were suppressed because of the zonal wind weakening after the onset.
276

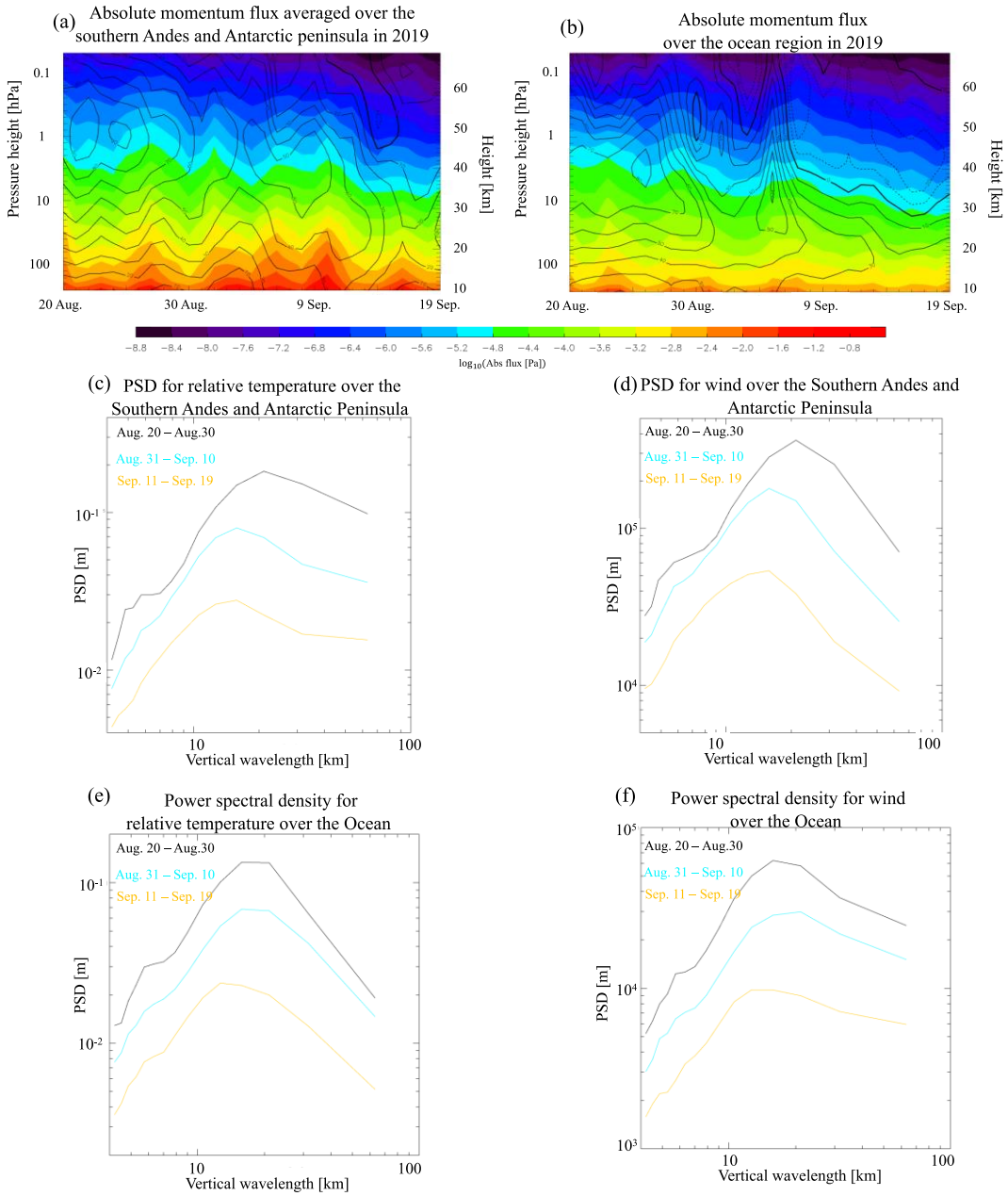

Figure 4 Graphs a and b show the daily mean absolute momentum fluxes in GEOS-5 FP over 50–80°W, 50–70°S (the southern Andes and Antarctic peninsula) and 165°E–165°W, 50–70°S (hereinafter, this region is called the ocean region). Graphs c and d show the vertical wavelength power spectral densities (PSDs) for the GW relative temperature and wind perturbation over the southern Andes and Antarctic peninsula in 10–70 km during August 20–30 (black), August 31–September 8 (blue), and September 9–19 (orange), respectively. Graphs e and f are the same as that in c, except over the ocean region.

5 Summary

We investigated GW variations before and after a rare Antarctic SSW event in 2019 using AIRS, AIM, and GEOS-5 FP. These results showed that the GW activity decreased after the SSW onset. The decrease coincided with the decrease in the zonal wind in GEOS-5 FP. In the GEOS-5 FP, the GW activity in the southern hemisphere decreased after the onset as a whole, except for the exit of the polar night jet. This temporal variation was the same as in the Arctic GWs in vortex displacement minor SSWs (Ern et al., 2016). Thus, the impact of vortex displacement SSWs on Antarctic GWs is similar to that in the Arctic, at least in the 2019 SSW event. The decrease in the GW activity after the onset was probably caused by wind filtering and polar night jet breaking. The GW activities over the Andes and Antarctic peninsula decreased by half at the SSW onset, although the zonal wind was still strong. This decrease could be caused by the shorter GW vertical wavelength because of zonal wind weakening. This result implied that the weakening zonal wind suppressed the GW momentum flux by half. Most previous studies regarding the SSW effect on GWs emphasized that a critical level is caused by wind reversal, but our results suggested that the effect of shortening the vertical wavelength cannot be negligible. These effects on the GWs because of the Antarctic SSW should change the GW activities and other phenomena in the upper atmosphere. In particular, this SSW could lower secondary GW excitation altitudes because of a descending primary GW breaking altitude, although GEOS-5 FP cannot resolve this type of secondary GW. Future work will investigate the impact of the decrease of the stratospheric GW on the upper atmosphere during the 2019 SSW.

Acknowledgments, Samples, and Data

This work was supported by the JSPS grant JRPs-LEAD with the DFG program, JSPS KAKENHI Grant Numbers 19K23465, 18H01270, 18H04446, and 17KK0095, and the Scientific Committee on Antarctic Research (SCAR) fellowship award 2019. We would like to thank Larry Coy (SSAI and NASA GSFC) for help accessing the GEOS5 FP data, Joan Alexander (NWRA) for providing the AIRS kernel function, Justin Carstens (Virginia Tech) and Cora Randall (CU) for providing the CIPS RAA kernel function. They also helped us to compare the GWs in both GEOS-5 FP and CIPS/AIM. The AIRS/Aqua gravity wave datasets (Hoffmann et al., 2017) are provided by Forschungszentrum Jülich (https://datapub.fz-juelich.de/slcs/airs/gravity_waves/data). The AIM/CIPS gravity wave datasets are provided by the University of Colorado

(http://lasp.colorado.edu/aim/download-data-raa.php). The GEOS-5 FP data were provided by NASA/GMAO (https://portal.nccs.nasa.gov/datashare/gmao/geos-fp/das/).

References

Alexander, M. J. (1998). Interpretations of observed climatological patterns in stratospheric gravity wave variance. *Journal of Geophysical Research* 103(D8), 8627– 8640. doi:10.1029/97JD03325

Alexander, S. P., Klekociuk, A. R., & Murphy, D. J. (2011). Rayleigh lidar observations of gravity wave activity in the winter upper stratosphere and lower mesosphere above Davis, Antarctica (69°S, 78°E). *Journal of Geophysical Research*116, D13109. doi:10.1029/2010JD015164

Aumann, H. H., Chahine, M. T., Gautier, C., Goldberg, M. D., Kalnay, E., McMillin, L. M., Revercomb, H., Rosenkranz, P. W., Smith, W. L., Staelin, D. H., Strow, L. L., & Susskind, J. (2003). AIRS/AMSU/HSB on the aqua mission: Design, science objectives, data products, and processing systems. *IEEE Transactions on Geoscience and Remote Sensing*, 41(2), 253–264. https://doi.org/10.1109/TGRS.2002.808356

Baldwin, M., Hirooka, T., & Oneill, A., & Yoden, S. (2003). Major stratospheric warming in the Southern Hemisphere in 2002: Dynamical aspects of the ozone hole split. *SPARC Newsletter*, 20, 24–26.

Bailey, S. M., Thomas, G. E., Rusch, D. W., Merkel, A. W., Jeppesen, C. D., Carstens, J. N., ... & Russell III, J. M. (2009). Phase functions of polar mesospheric cloud ice as observed by the CIPS instrument on the AIM satellite. *Journal of Atmospheric and Solar-Terrestrial Physics*, 71(3–4), 373–380. https://doi.org/10.1016/j.jastp.2008.09.039

Carstens, J. N., S. M. Bailey, J. D. Lumpe, & C. E. Randall. (2013). Understanding uncertainties in the retrieval of polar mesospheric clouds from the cloud imaging and particle size experiment in the presence of a bright Rayleigh background, *Journal of Atmospheric and Solar-Terrestrial Physics*., 104, 197–212. doi:10.1016/j.jastp.2013.08.006

Chahine, M. T., Pagano, T. S., Aumann, H. H., Atlas, R., Barnet, C., Blaisdell, J., Chen, L., Divakarla, M., Fetzer, E. J., Goldberg, M., Gautier, C., Granger, S., Hannon, S., Irion, F. W., Kakar, R., Kalnay, E., Lambrigtsen, B. H., Lee, S.-Y., Le Marshall, J., Mcmillan, W. W., Mcmillin, L., Olsen, E. T., Revercomb, H., Rosenkranz, P., Smith, W. L., Staelin, D.,

Strow, L. L., Susskind, J., Tobin, D., Wolf, W., & Zhou, L. (2006). AIRS: Improving weather forecasting and providing new data on greenhouse gases *Bulletin of the American Meteorological Society*, 87(7), 911– 926. https://doi.org/10.1175/BAMS-87-7-911

Chandran, A., Collins, R. L., & Harvey, V. L. (2014). Stratosphere–mesosphere coupling during stratospheric sudden warming events. *Advances in Space Research*, 53(9), 1265–1289. https://doi.org/10.1016/j.asr.2014.02.005

Charlton, A. J., & Polvani, L. M. (2007). A new look at stratospheric sudden warmings. Part I: Climatology and modeling benchmarks. *Journal of Climate*, 20, 449–469. https://doi.org/10.1175/JCLI3996.1

Ern, M., Trinh, Q. T., Kaufmann, M., Krisch, I., Preusse, P., Ungermann, J., Zhu, Y., Gille, J. C., Mlynczak, M. G., Russell III, J. M., Schwartz, M. J., & Riese, M. (2016). Satellite observations of middle atmosphere gravity wave absolute momentum flux and of its vertical gradient during recent stratospheric warmings. *Atmospheric Chemistry and Physics*, 16, 9983–10019. https://doi.org/10.5194/acp-16-9983-2016

Fleming, E. L., Chandra, S., Barnett, J. J., & Corney, M. (1990). Zonal mean temperature, pressure, zonal wind, and geopotential height as functions of latitude. *Advances in Space Research*, 10(12), 11–59. https://doi.org/10.1016/0273-1177(90)90386-E

Fritts, D. C. & Alexander, M. J. (2003). Gravity wave dynamics and effects in the middle atmosphere. Reviews of Geophysics, 41, 1003, doi:10.1029/2001RG000106, 1

Gelaro, R., & Coauthors. (2017). The modern-era retrospective analysis for research and applications, Version 2 (MERRA-2). *Journal of Climate*, 30, 5419–5454. https://doi.org/10.1175/JCLI-D-16-0758.1

Garcia, R. R., & Boville, B. A. (1994). "Downward control" of the mean meridional circulation and temperature distribution of the polar winter stratosphere. *Journal of Atmospheric Science*, 51, 2238–2245. https://doi.org/10.1175/1520-0469(1994)051<2238:COTMMC>2.0.CO;2

Geller, M. A., & coauthors (2013) A comparison between gravity wave momentum fluxes in observations and climate models. *Journal of Climate*, 26, 6383–6405. https://doi.org/10.1175/JCLI-D-12-00545.1

Geller, M. A. & Gong, J. (2010). Gravity wave kinetic, potential, and vertical fluctuation energies as indicators of different frequency gravity waves. *Journal of Geophysical Research*, 115, D11111. doi:10.1029/2009JD012266

Hendricks, E. A., J. D. Doyle, S. D. Eckermann, Q. Jiang, & P. A. Reinecke. (2014) What Is the Source of the Stratospheric Gravity Wave Belt in Austral Winter? *Journal of Atmospheric Science*, 71, 1583–1592. https://doi.org/10.1175/JAS-D-13-0332.1

Hoffmann, L., Spang, R., Orr, A., Alexander, M. J., Holt, L. A., & Stein, O. (2017). A decadal satellite record of gravity wave activity in the lower stratosphere to study polar stratospheric cloud formation. *Atmospheric Chemistry and Physics*, 17(4), 2901–2920. https://doi.org/10.5194/acp-17-2901-2017

Hoffmann, L., Xue, X., & Alexander, M. J. (2013). A global view of stratospheric gravity wave hotspots located with atmospheric infrared sounder observations. *Journal of Geophysical Research: Atmospheres*, 118, 416–434. https://doi.org/10.1029/2012JD018658

Holt, L. A., Alexander, M. J., Coy, L., Molod, A., Putman, W., Pawson, S. (2016). Tropical Waves and the Quasi-Biennial Oscillation in a 7-km Global Climate Simulation. J. Atmos. Sci., 73, 3771–3783, https://doi.org/10.1175/JAS-D-15-0350.1.

Holt, L.A., Alexander, M.J., Coy, L., Liu, C., Molod, A., Putman, W. & Pawson, S. (2017), An evaluation of gravity waves and gravity wave sources in the Southern Hemisphere in a 7 km global climate simulation. *Q.J.R. Meteorol. Soc*, 143: 2481-2495. https://doi.org/10.1002/qj.3101

Jewtoukoff, V., A. Hertzog, R. Plougonven, A. D. L. Cámara, and F. Lott, (2015). Comparison of Gravity Waves in the Southern Hemisphere Derived from Balloon Observations and the ECMWF Analyses. *Journal of Atmospheric Science*, 72, 3449–3468. https://doi.org/10.1175/JAS-D-14-0324.1

Jia, Y., Zhang, S. M., Yi, F., Huang, C. M., Huang, K. M., Gan, Q., & Gong, Y. (2015) Observations of gravity wave activity during stratospheric sudden warmings in the Northern Hemisphere. *Science China Technological Sciences*, 58, 951–960. https://doi.org/10.1007/s11431-015-5806-3

Lindzen, R. S. (1981). Turbulence and stress owing to gravity wave and tidal breakdown *Journal of Geophysical Research*, 86 (C10), 9707–9714. doi:10.1029/JC086iC10p09707

Lucchesi, R. (2013). File specification for GEOS-5 FP, *Tech. Rep. GMAO Off. Note No. 4 (Version 1.0)*, Available at https://ntrs.nasa.gov/search.jsp?R=20150001437

Matthewman, N. J., Esler, J. G., Charlton-Perez, A. J., & Polvani, L. M. (2009). A new look at stratospheric sudden warmings. Part III: Polar vortex evolution and vertical structure, *Journal of Climate*, 22, 1566–1585. https://doi.org/10.1175/2008JCLI2365.1

McClintock, W. E., Rusch, D. W., Thomas, G. E., Merkel, A. W., Lankton, M. R., Drake, V. A., ... & Russell III, J. M. (2009). The cloud imaging and particle size experiment on the aerosol of ice in the mesosphere mission: Instrument concept, design, calibration, and on-orbit performance. *Journal of Atmospheric and Solar-Terrestrial Physics*, 71(3–4), 340–355. https://doi.org/10.1016/j.jastp.2008.10.011

McFarlane, N. A. (1987). The effect of orographically excited gravity wave drag on the general circulation of the lower stratosphere and troposphere. *Journal of Atmospheric Science*, 44, 1775–1800. https://doi.org/10.1175/1520-0469(1987)044<1775:TEOOEG>2.0.CO;2

Murphy, D. J., Alexander, S. P., Klekociuk, A. R., Love, P. T., & Vincent, R. A. (2014). Radiosonde observations of gravity waves in the lower stratosphere over Davis, Antarctica. *Journal of Geophysical Research: Atmospheres*, 119, 11,973–11,996, doi:10.1002/2014JD022448

Plougonven, R., & Zhang, F. (2014). Internal gravity waves from atmospheric jets and fronts. *Reviews of Geophysics*, 52, 33–76, doi:10.1002/2012RG000419

Preusse, P., Eckermann, S. D., Ern, M., Oberheide, J., Picard, R. H., Roble, R. G., Riese, M., Russell, J. M., & Mlynczak, M. G. (2009). Global ray tracing simulations of the SABER gravity wave climatology. *Journal of Geophysical Research*, 114, D08126, doi:10.1029/2008JD011214

Randall, C. E., Carstens, J., France, J. A., Harvey, V. L., Hoffmann, L., Bailey, S. M., Alexander, M. J., Lumpe, J. D., Yue, J., Thurairajah, B., Siskind, D. E., Zhao, Y., Taylor, M. J., and Russell, III, J. M.. (2017). New AIM/CIPS global observations of gravity waves near 50–55 km. *Geophysical Research Letters*, 44, 7044–7052, doi:10.1002/2017GL073943

Ratnam, M. V., Tetzlaff G., & Jacobi C. (2004). Global and seasonal variations of stratospheric gravity wave activity deduced from the CHAMP/GPS satellite. *Journal of Atmospheric Science*, 61, 1610–1620. https://doi.org/10.1175/1520-0469(2004)061<1610:GASVOS>2.0.CO;2

435 Rusch, D., Thomas, G., Merkel, A., Olivero, J., Chandran, A., Lumpe, J., & Russell III, J. (2017).
436 Large ice particles associated with small ice water content observed by AIM CIPS
437 imagery of polar mesospheric clouds: Evidence for microphysical coupling with small-
438 scale dynamics. *Journal of Atmospheric and Solar-Terrestrial Physics*, 162, 97–105.
439 doi:10.1016/j.jastp.2016.04.018
440 Scargle, J. D. (1982). Studies in astronomical time series analysis II. Statistical aspects of spectral
441 analysis of unevenly spaced data. *The Astrophysical Journal*, 263, 835.
442 doi:10.1086/160554
443 Sato & Yoshiki, M. (2008). Gravity wave generation around the polar vortex in the stratosphere
444 revealed by 3-hourly radiosonde observations at Syowa Station. *Journal of the*
445 *Atmospheric Sciences*, 65(12), 3719–3735. Retrieved Dec. 29, 2020,
446 doi:10.1175/2008JAS2539.1
447 Thurairajah, B., Bailey, S. M., Cullens, C. Y., Hervig, M. E., & Russell III, J. M. (2014). Gravity
448 wave activity during recent stratospheric sudden warming events from SOFIE
449 temperature measurements. *Journal of Geophysical Research: Atmospheres*, 119, 8091–
450 8103. doi:10.1002/2014JD021763
451 Wang, L., & Alexander, M. J. (2009). Gravity wave activity during stratospheric sudden warmings
452 in the 2007–2008 Northern Hemisphere winter. *Journal of Geophysical Research*, 114,
453 D18108. doi:10.1029/2009JD011867
454 Whiteway, J. A., Duck, T. J., Donovan, D. P., Bird, J. C., Pal, S. R., & Carswell, A. I. (1997).
455 Measurements of gravity wave activity within and around the Arctic stratospheric vortex,
456 *Geophysical Research Letters*, 24(11), 1387– 1390. doi:10.1029/97GL01322
457 Wright, C. J., Osprey, S. M., Barnett, J. J., Gray, L. J., & Gille, J. C. (2010). High resolution
458 dynamics limb sounder measurements of gravity wave activity in the 2006 Arctic
459 stratosphere. *Journal of Geophysical Research*, 115, D02105,
460 doi:10.1029/2009JD011858
461 Yamashita, C., England, S. L., Immel, T. J., & Chang, L. C. (2013). Gravity wave variations during
462 elevated stratopause events using SABER observations. *Atmospheres*, 118, 5287–5303.
463 doi:10.1002/jgrd.50474

Yamashita, C., Liu, H.-L., & Chu, X. (2010). Gravity wave variations during the 2009 stratospheric sudden warming as revealed by ECMWF-T799 and observations, *Geophysical Research Letters*, 37, L22806. doi:10.1029/2010GL045437

Yamazaki, Y., Matthias, V., Miyoshi, Y., Stolle, C., Siddiqui, T., & Kervalishvili, G., et al. (2020). September 2019 Antarctic sudden stratospheric warming: Quasi-6-day wave burst and ionospheric effects. *Geophysical Research Letters*, 47, e2019GL086577. https://doi.org/10.1029/2019GL086577